Prepared for submission to JHEP

Updating Fifth-force Constraints from Juno Mission

Eashan Iyer,[a] Ash Lassonde,[a] Praniti Singh[a] and JiJi Fan[a]

[a] *Department of Physics, Brown University*

E-mail: eashan_iyer@brown.edu, ash_lassonde@brown.edu, praniti_singh@brown.edu, jiji_fan@brown.edu

Abstract: The orbits of celestial bodies have long served as laboratories for fundamental physics: the anomalous precession of Mercury's orbit famously provided early evidence for general relativity. Today, spacecraft orbits offer the same opportunity with far greater precision. NASA's Juno probe has orbited Jupiter since 2016 on a highly elliptical path, sweeping from just above the planet's cloud tops to millions of kilometers away. This makes its motion exceptionally sensitive to any theoretical long-range fifth force between Juno and Jupiter, beyond the four known fundamental interactions. Such a force would cause Juno's orbit to precess slightly more than gravity alone predicts. Requiring that this extra precession remain within the uncertainty of Jupiter's measured gravitational field places limits on the strength of the force as a function of its range.

We update our group's previous constraint using an improved determination of the Jovian gravitational field, which benefits both from the many additional orbits Juno has completed and from physically motivated assumptions about Jupiter's atmospheric winds. Our results demonstrate that ongoing refinements in planetary gravity measurements translate into stronger tests of physics beyond the Standard Model.

Contents

1 Introduction

Precise measurements of orbital motion provide a powerful test of fundamental physics. Historically, discrepancies between observed orbits and the predictions of established gravitational models have revealed new phenomena, including the existence of Neptune and evidence for general relativity. Spacecraft extend this methodology to controlled probes whose trajectories can be measured with exceptional accuracy.

NASA's Juno spacecraft is particularly well suited to such a test. Launched in 2011 and inserted into orbit around Jupiter in 2016, Juno follows a highly eccentric, nearly polar, trajectory that carries it from around 4,000 km above the planet to 8.1 million km away between successive perijoves [1]. Radio tracking of this motion has enabled precise measurements of Jupiter's gravitational field, as discussed in Sec. 3.

Although Juno was designed primarily to investigate Jupiter's origin, interior, atmosphere, and magnetosphere, its orbit also makes the mission a laboratory for physics beyond the Standard Model (BSM). After the known gravitational and nongravitational influences on the spacecraft have been modeled, the remaining uncertainty in its motion can be used to constrain an additional interaction between Juno and Jupiter.

A sufficiently light scalar or vector particle could mediate a long-range interaction, commonly called a fifth force. Because Juno repeatedly moves between a close perijove and distant apojove, the strength of a finite-range interaction could vary substantially along its orbit and produce an additional precession of its periapsis. This basic premise is illustrated schematically in Fig. 1.

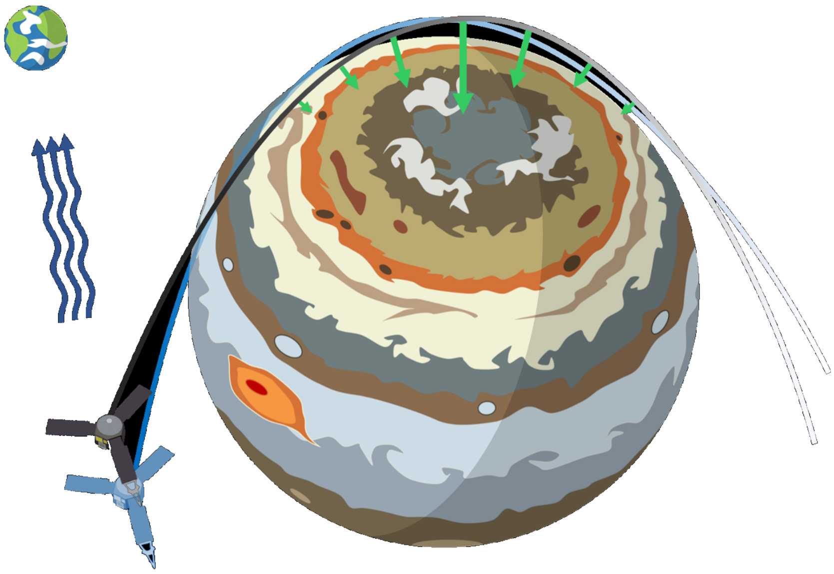

Figure 1. Diagram of the premise of our test. Juno's highly eccentric orbit carries it through regions in which a finite-range fifth force sourced by Jupiter can differ greatly in strength. The green arrows represent the additional force along the trajectory, while the light-blue curve illustrates a possible perturbed orbit. Reproduced from Ref. [2] with permission from the authors.

Singh et al. first developed this idea into a constraint on long-range new physics using Juno's orbit [2]. They parameterized the additional interaction using a Yukawa potential, calculated the resulting periapsis precession, and compared it with the uncertainty produced by the measured Jovian gravitational field. Requiring the additional precession to remain within this uncertainty gave constraints on the possible strength and range of the interaction.

The previous analysis used the gravity solution reported by Durante et al. [3]. In this update, we instead use the newer solution of Kaspi et al., which incorporates additional Juno observations and a revised treatment of Jupiter's high-degree gravity field [4]. The data underlying these solutions and the specific improvements in the Kaspi analysis are described in Sec. 3.

We retain the theoretical framework of Ref. [2] but propagate the updated gravity covariance into the uncertainty in Juno's periapsis precession. We then translate this revised uncertainty into an updated exclusion in fifth-force strength and range. This comparison demonstrates how refinements made for planetary science can simultaneously sharpen tests of BSM physics without requiring a new instrument or a dedicated fifth-force mission.

The remainder of this paper is organized as follows. Section 2 introduces the fifth-force parameterization, the Jovian gravitational harmonics, and the precession observable. Section 3 describes the gravity data and the differences between the Durante and Kaspi analyses. Section 4 presents the covariance propagation and confidence criterion. Sections 6 and 7 present the updated constraints and discuss their interpretation, limitations, and possible extensions.

2 Theoretical Framework

2.1 Fifth-force parameterization

A wide range of BSM theories introduce a new light scalar or vector particle that couples to ordinary matter. At nonrelativistic energies, exchanging a massive particle between two objects produces a Yukawa potential. This form can be understood as the massive analogue of the familiar $1/r$ potential: the massless-field equation gives a $1/r$ solution, while the mass term causes the field to be exponentially suppressed beyond the mediator's Compton wavelength. For point objects of masses M and m, we therefore parameterize the additional potential energy as [2, 5]

$$U_{\text{point}}(r) = -\alpha \frac{GMm}{r} e^{-r/\lambda}, \tag{2.1}$$

where r is their separation, G is the gravitational constant, α is the strength of the new interaction relative to gravity, and λ is its range. The corresponding mediator mass is

$$m_* = \frac{\hbar c}{\lambda}. \tag{2.2}$$

With the convention in Eq. (2.1), positive α describes an attractive interaction and negative α a repulsive one. If the two objects carry fifth-force charges Q and q and the new coupling is g, then

$$\alpha = \pm \frac{g^2 Qq}{4\pi GMm}. \tag{2.3}$$

The value of α therefore depends on both the underlying particle-physics model and the composition of the two bodies.

This parameterization covers several well-motivated possibilities without requiring the analysis to be repeated for each one. Examples include new gauge bosons associated with gauged baryon number $U(1)_B$, baryon number minus lepton number $U(1)_{B-L}$, or differences between lepton-flavor numbers, as well as light scalar particles coupled to baryons [2, 6–9]. Yukawa corrections can also arise in modified-gravity theories. The parameters (α, λ)

provide a common phenomenological description of these scenarios: a bound in this plane can be translated into a model-specific bound once the charges and coupling in Eq. (2.3) are specified.

2.2 The finite size of Jupiter

Equation (2.1) treats Jupiter as a point mass. This is insufficient when the force range is comparable to Jupiter's radius, because different parts of the planet are separated from Juno by different distances and are therefore weighted differently by the exponential factor. Following Ref. [2], the point-source potential is replaced by an integral over Jupiter's volume,

$$U_5(\mathbf{r}) = -\alpha G m_{\mathrm{J}} \int_{V_{\mathrm{J}}} \frac{\rho(\mathbf{r}')}{|\mathbf{r}-\mathbf{r}'|} \exp\left[-\frac{|\mathbf{r}-\mathbf{r}'|}{\lambda}\right] d^3\mathbf{r}', \tag{2.4}$$

where m_{J} is the mass of the Juno spacecraft, $\mathbf{r}$ is its position relative to Jupiter's center, and $\rho(\mathbf{r}')$ is Jupiter's mass density. We use the same spherically symmetric, two-layer density profile as Ref. [2], taken from the interior models of Militzer and Hubbard [10]. Juno is treated as a point object because its physical dimensions are negligible on the relevant length scales.

Equation (2.4) assumes that Jupiter's fifth-force charge density is proportional to its mass density, with the overall charge-to-mass ratio absorbed into α. This is appropriate, for example, for an interaction coupled approximately to baryon number. For a model such as $U(1)_{B-L}$, the source instead depends on the local composition and the integral must be modified accordingly. The spherical approximation also neglects smaller corrections to the fifth-force source from Jupiter's oblate shape and nonspherical density distribution. Ref. [2] estimates that these corrections change the resulting constraint by no more than order 10^{-2}, so they are subleading at the precision considered here.

The finite-size treatment is most important when λ is comparable to or smaller than the Jovian radius. In that regime, material on the side of Jupiter nearest Juno contributes more strongly than material near the center or far side, so the extended planet cannot be replaced by a mass concentrated at its center. At ranges much larger than the radius, Eq. (2.4) approaches the point-source result.

2.3 Gravitational harmonics and orbital precession

The conventional gravitational field must also account for the fact that Jupiter is neither spherical nor uniform. The effective potential for this field can be written as a spherical Newtonian term plus a relativistic correction and a series of zonal harmonics [2]:

$$V(r,z) = \frac{\mu}{r}\left[1 + \frac{\mu a(1-e^2)}{c^2 r^2} - \sum_{\ell=2}^{\infty} \left(\frac{R_{\mathrm{J}}}{r}\right)^{\ell} J_\ell P_\ell\left(\frac{z}{r}\right)\right]. \tag{2.5}$$

Here $\mu = GM_{\mathrm{Jup}}$, R_{J} is Jupiter's reference radius, a and e are Juno's semimajor axis and eccentricity, c is the speed of light, z is the spacecraft's distance from Jupiter's equatorial plane, and P_ℓ is a Legendre polynomial. The dimensionless coefficients J_ℓ describe how the measured field differs from that of a spherical point mass. Jupiter's rapid rotation and oblate shape produce a particularly large J_2, while the higher-degree terms encode progressively finer structure arising from the planet's internal density distribution and atmospheric dynamics.

Only the zonal, or longitude-independent, harmonics are retained in Eq. (2.5). This is the appropriate leading description because the fifth force is taken to be spherically symmetric and the tracking data span many rotations of Jupiter and its major moons. The fitted J_ℓ values are not known exactly, however, and their errors are correlated. As a result, the conventional gravity model permits a range of possible perturbations to Juno's orbit. The updated covariance of these coefficients is the central data input to our analysis and is discussed in Sec. 3.

We characterize the orbital response using the argument of periapsis ω, the angle locating Juno's closest approach within its orbital plane. In an ideal Newtonian $1/r$ potential, an orbit closes after each revolution and ω does not accumulate a secular shift. General relativity, the nonspherical Jovian field, and a Yukawa interaction all perturb the inverse-square force and cause the periapsis to drift. Precession is therefore useful because it collects a small acceleration acting throughout an orbit into a cumulative, physically interpretable change in an orbital element.

At leading order the fifth force is a radial perturbation. The Gauss planetary equation gives its contribution to the instantaneous precession rate as [2, 11]

$$\dot{\omega}_5 = -\sqrt{\frac{a(1-e^2)}{e^2\mu}}\,\frac{1}{m_{\rm J}}\,\frac{\partial U_5}{\partial r}\cos f, \tag{2.6}$$

where f is the true anomaly measured from perijove. Averaging over a complete orbit gives

$$\langle \Delta\omega_5\rangle = \frac{1}{2\pi}\int_0^{2\pi}\frac{\dot{\omega}_5}{h/r^2}\,df, \qquad r(f) = \frac{a(1-e^2)}{1+e\cos f}, \tag{2.7}$$

where h is the orbital angular momentum per unit mass. These equations are evaluated numerically using the finite-size potential in Eq. (2.4); the full derivation is given in Ref. [2].

For a fixed range, the predicted shift is proportional to α. Its dependence on λ is not monotonic. If the force range is much shorter than the distances sampled by Juno, the exponential suppression makes the effect negligible. If the range is much longer than the orbit, the leading part of the interaction resembles an additional $1/r$ potential and produces little distinguishable precession. The sensitivity is therefore greatest at intermediate ranges comparable to the characteristic scale of Juno's motion around Jupiter. The next sections describe how the uncertainty in the standard gravitational contribution to the same observable is inferred from the Juno data and used to decide which values of (α, λ) remain allowed.

3 Jovian Gravitational Field Data Updates

3.1 Source of the gravity data

Jupiter's gravitational harmonics are inferred from radio tracking of the Juno spacecraft. An antenna in NASA's Deep Space Network transmits radio signals to Juno, which then retransmits them to Earth. The Doppler shifts of these signals are measured and then processed to infer the dynamics of the space probe. Two frequencies are used to reduce the dispersive noise introduced by charged particles along the signal path [3].

The Doppler measurements are then compared with the motion predicted by a detailed model of Juno's orbit. This model includes the gravitational influence of Jupiter and its satellites, Jupiter's nonspherical gravity field, tides, relativistic effects, solar radiation pressure, and small empirical accelerations acting on the spacecraft. A joint least-squares fit across multiple perijove passes estimates both parameters specific to each orbit and parameters shared by all of the orbits. The shared parameters include Jupiter's gravitational harmonics J_ℓ.

Because these parameters are not independent, the fit also produces a covariance matrix describing the uncertainties in the J_ℓ and the correlations between them. Since we are working with uncertainties rather than the values of these harmonics, this covariance matrix is the principal data source for our analysis.

3.2 The Durante and Kaspi gravity solutions

The previous fifth-force analysis used the gravity solution of Durante et al., which combined radio-tracking data from 10 perijove passes collected during the first half of Juno's nominal mission [2, 3]. Durante et al. estimated Jupiter's zonal gravitational harmonics through degree 30, together with the other orbital and physical parameters required by their model. This solution represented a substantial improvement over the gravity field inferred from Juno's first two passes, but the limited number and geometry of the available observations left significant correlations among some of the fitted harmonics.

Kaspi et al. subsequently analyzed 26 perijove datasets extending from PJ01 in August 2016 through PJ37 in October 2021 [4] [1]. The additional passes provide more measurements of Juno's response to the same underlying Jovian gravity field. They also sample a wider range of perijove locations as Juno's closest approach shifts northward during the mission. Because the gravitational coefficients are common to all of the orbital arcs, fitting more passes provides additional information with which to separate their individual contributions.

The main differences between the two gravity solutions are summarized in Table 1 and discussed below in more detail.

A second difference is the use of physically motivated spatial constraints at high latitudes. Juno approaches Jupiter most closely at low and middle latitudes and is therefore considerably less sensitive to short-wavelength gravity structure near the poles. The previous unconstrained global fit had useful sensitivity only through approximately J_{12}. Kaspi et al. observe that Jupiter's high-latitude zonal winds are relatively weak and that the static interior is not expected to contribute significantly to the gravity spectrum at high degree; they therefore constrain the contribution to the surface acceleration produced by J_{13} through J_{40} to remain small in the poorly sampled polar regions. The total surface acceleration does depend on the low-degree coefficients, but these coefficients are not included

[1] Durante's data is publicly available as a part of their publication, which Kaspi's data was obtained through private correspondence.

	Durante et al. (2020)	Kaspi et al. (2023)
Data coverage	10 gravity data sets spanning PJ01–PJ17	26 perijove data sets spanning PJ01–PJ37
Zonal expansion	Harmonics fitted through J_{30}	Harmonics fitted through J_{40}
High-degree treatment	Coefficients above approximately J_{12} are strongly correlated and not reliably determined	Spatial/atmospheric constraints lead to more reliable determinations of J_{13}–J_{40}, motivated by the weak high-latitude winds

Table 1. Comparison of the Jovian gravity solutions used in the previous and updated fifth-force analyses.

in the spatial constraint and continue to describe Jupiter's global zonal gravity field. This reduces the degeneracy among the high-degree coefficients and allows the gravity field to be resolved primarily over the latitude range where Juno has the greatest sensitivity. This introduces model dependence into the analysis; however, this dependence is well motivated, and the low-degree coefficients that have large impacts on the final result are less affected by it than the high-degree coefficients.The third difference is the extension of the fitted zonal-harmonic expansion from degree 30 to degree 40, leading to a larger covariance matrix with which to propagate the uncertainty in the probe's precession. Kaspi et al. tested the stability of these coefficients using multiple subsets of the perijove data and enlarged the formal uncertainties of J_{13} through J_{40} where necessary to encompass the variation between the resulting solutions [4].

The second and third improvements are closely related: the extension to J_{40} is possible largely because the atmospheric model makes those higher-degree coefficients distinguishable. These changes produce a covariance matrix that is both more precise and structurally different from the one used in Ref. [2]. In Sec. 4, we describe how this covariance is propagated into the uncertainty in Juno's periapsis precession.

4 Methodology

4.1 From the gravity solution to a precession uncertainty

The theoretical framework in Sec. 2 predicts two contributions to Juno's periapsis precession. A fifth force produces an additional shift $\langle \Delta\omega_5(\alpha, \lambda)\rangle$, while uncertainty in the conventional Jovian gravity field permits a range of shifts $\langle \Delta\omega_g\rangle$. The purpose of the analysis is to determine whether a predicted fifth-force shift is small enough to be consistent with Juno's gravitational uncertainty.

The parameters collected from the gravitational fit are assembled into the vector

$$\mathbf{p} = (\mu, J_2, J_3, \ldots, J_N)\,, \tag{4.1}$$

where N is the maximum harmonic degree included in the calculation. The precession can therefore be written with the following dependencies:

$$\langle \Delta\omega_g\rangle = \langle \Delta\omega_g\rangle\,(\mathbf{p}; a, e, i, \omega), \tag{4.2}$$

where (a, e, i, ω) specify the orbital geometry. The derivatives of this quantity with respect to the gravity parameters define the sensitivity vector

$$\mathbf{g} \equiv \frac{\partial \langle \Delta\omega_g \rangle}{\partial \mathbf{p}}. \tag{4.3}$$

These derivatives are evaluated using the Gauss planetary equations described in Sec. 2. Singh et al. calculate them through J_10, and we extend them numerically through J_{40}.

The gravity analyses of Durante et al. and Kaspi et al. provide not only estimates of the J_ℓ, but also covariance matrices describing their uncertainties and correlations [3, 4]. For a covariance matrix $\mathbf{C}$ expressed in the same coefficient basis as $\mathbf{g}$, standard linear uncertainty propagation gives

$$\sigma_\omega^2 = \mathbf{g}^{\mathrm{T}} \mathbf{C} \mathbf{g}. \tag{4.4}$$

This quantity is the variance of the conventional periapsis shift allowed by the gravity solution. The full covariance matrix is required in Eq. (4.4), since treating the harmonic uncertainties independently would be invalid because of the correlations between gravitational coefficients.

The dependence of $\mathbf{g}$ on i and ω means that σ_ω is not a property of the gravity solution alone. It also depends on the geometry of the particular Juno orbit being considered. We evaluate Eq. (4.4) at the first-perijove benchmark,

$$i \simeq 1.57, \qquad \omega \simeq 3.08, \tag{4.5}$$

used in Ref. [2] to directly benchmark our result against existing literature, and then separately over the range of orbits sampled by the mission.

4.2 Covariance normalization

Care is required because the two covariance matrices are expressed using different conventions. The Durante covariance is stored in terms of fully normalized coefficients

$$\bar{J}_\ell = \frac{J_\ell}{\sqrt{2\ell + 1}}, \tag{4.6}$$

whereas the re-derived covariance associated with the Kaspi solution is expressed directly in terms of the unnormalized J_ℓ. This identification is verified by comparing the square roots of the covariance diagonals with the uncertainties reported in the corresponding gravity tables.

The gradient must be transformed with the covariance. From Eq. (4.6),

$$\frac{\partial \langle \Delta\omega_g \rangle}{\partial \bar{J}_\ell} = \sqrt{2\ell + 1}\, \frac{\partial \langle \Delta\omega_g \rangle}{\partial J_\ell}. \tag{4.7}$$

We therefore contract the Durante covariance with the normalized gradient in Eq. (4.7), and the Kaspi covariance with the unnormalized gradient. Contracting both matrices with the same raw gradient would mix coefficient conventions and artificially enlarge the apparent improvement.

The contribution associated with the uncertainty in μ is negligible, and we observed that removing it changes σ_ω by $1.4 \times 10^{-4}\%$. We therefore use the J_ℓ covariance blocks in the comparisons below.

4.3 Diagonal and correlated contributions

To determine whether the improvement comes from smaller individual uncertainties or from changes in the correlations, we decompose Eq. (4.4) as

$$\sigma_\omega^2 = \underbrace{\sum_\ell g_\ell^2 C_{\ell\ell}}_{\sigma^2_{\rm diag}} + \underbrace{\sum_{\ell\neq\ell'} g_\ell g_{\ell'} C_{\ell\ell'}}_{\sigma^2_{\rm off}}, \tag{4.8}$$

where $g_\ell = \partial\langle\Delta\omega_g\rangle/\partial J_\ell$. The first term contains the individual harmonic variances, while the second contains all covariance terms. The quantity $\sigma^2_{\rm off}$ can either increase or decrease the total propagated variance, as it can be negative, unlike the diagonal terms. We report the signed fractional shift in terms of the standard deviation:

$$\delta_{\rm corr} = \frac{\sigma_\omega - \sigma_{\rm diag}}{\sigma_\omega}. \tag{4.9}$$

4.4 Fifth-force exclusion criterion

For a fixed force range, the fifth-force precession is linear in α. We therefore write

$$\langle\Delta\omega_5(\alpha,\lambda)\rangle = \alpha\,\mathcal{F}(\lambda), \tag{4.10}$$

where $\mathcal{F}(\lambda)$ is calculated numerically using the finite-size Jovian density integral in Eq. (2.4). The gravity solution is treated as consistent with no detected anomalous precession. Following Ref. [2], we impose a two-σ confidence interval, corresponding to approximately 95%:

$$|\langle\Delta\omega_5(\alpha,\lambda)\rangle| \leq 2\sigma_\omega. \tag{4.11}$$

The limiting fifth-force strength for a given range can be expressed as the following function of λ:

$$|\alpha|_{95}(\lambda) = \frac{2\sigma_\omega}{|\mathcal{F}(\lambda)|}. \tag{4.12}$$

Values with $|\alpha| > |\alpha|_{95}$ correspond to a precession inconsistent with Juno's observed precession uncertainty and can therefore be excluded under our criterion.

5 Intermediate Results

5.1 Reproduction of the previous calculation

We first validate the numerical pipeline by reproducing the calculation of Ref. [2]. Using the Durante covariance, the rounded first-perijove geometry $i = 1.57$ and $\omega = 3.08$, and harmonics through J_{10}, we obtain

$$\sigma_\omega = 9.33 \times 10^{-10} \tag{5.1}$$

when the covariance is contracted using the convention employed in the original analysis. This agrees with the approximate value of 9.0×10^{-10} observed in that plot. The numerical derivatives also reproduce the analytic expressions through J_{10} to numerical precision.

This reproduction verifies the orbital and covariance-propagation calculations. For the quantitative comparison between the old and updated gravity solutions, however, we use the basis-consistent treatment described in Sec. 4. This distinction is necessary because the two covariance products are not expressed in the same harmonic basis.

5.2 Dependence on harmonic degree

The updated result is dominated by the lowest-degree harmonic. Using only J_2 gives

$$\sigma_\omega(J_2) = 1.74 \times 10^{-9}, \tag{5.2}$$

while including the complete updated covariance through J_{40} gives

$$\sigma_\omega(J_2, \ldots, J_{40}) = 1.74 \times 10^{-9}. \tag{5.3}$$

All degrees above J_2 therefore change the total uncertainty by only approximately 0.1%. The curve is effectively converged by $N = 4$, despite the availability of coefficients through J_{40}.

The reason for this behavior is that the derivatives $\partial\langle\Delta\omega_g\rangle/\partial J_\ell$ decrease rapidly with increasing degree. The updated covariance keeps the uncertainties of the high-degree coefficients sufficiently controlled so that this decrease is not offset by rapidly increasing variances or strong correlations between terms. As a result, the precession observable is overwhelmingly sensitive to J_2.

This is not the case in the prior calculation, whose basis-consistent uncertainty grows from 1.80×10^{-9} using J_2 alone to 2.33×10^{-9} through J_{30} and does not fully plateau until approximately $N = 12$. The larger high-degree uncertainties and their covariance structure therefore contribute materially to the previously calculated error.

5.3 Role of harmonic correlations

The diagonal-only standard deviations through $N = 30$ are

$$\sigma_{\rm diag}^{\rm Durante} = 2.06 \times 10^{-9}, \qquad \sigma_{\rm diag}^{\rm Kaspi} = 1.85 \times 10^{-9}. \tag{5.4}$$

Including the covariance terms raises the Durante result to 2.33×10^{-9} but lowers the updated result to 1.74×10^{-9}. In terms of Eq. (4.9), the correlations increase the Durante standard deviation by approximately 11.6%, whereas they decrease the updated standard deviation by approximately 6.3%. Equivalently, the off-diagonal terms account for approximately +21.9% of the Durante variance and −13.0% of the updated variance.

The Durante covariance exhibits a strong alternating-sign structure. Neighboring degrees are increasingly anticorrelated, reaching correlation coefficients close to −1 at intermediate and high degree. Because the precession derivatives also alternate in sign, many of the resulting cross terms are positive and add constructively to the propagated variance.

The updated covariance has weaker and less regularly alternating correlations among the low-degree coefficients. Strong correlations remain among some high-degree terms, but they appear where the corresponding precession derivatives are already small. Their net contribution is mildly destructive rather than constructive. The improvement is therefore not explained solely by smaller diagonal uncertainties: the changed correlation structure is also essential.

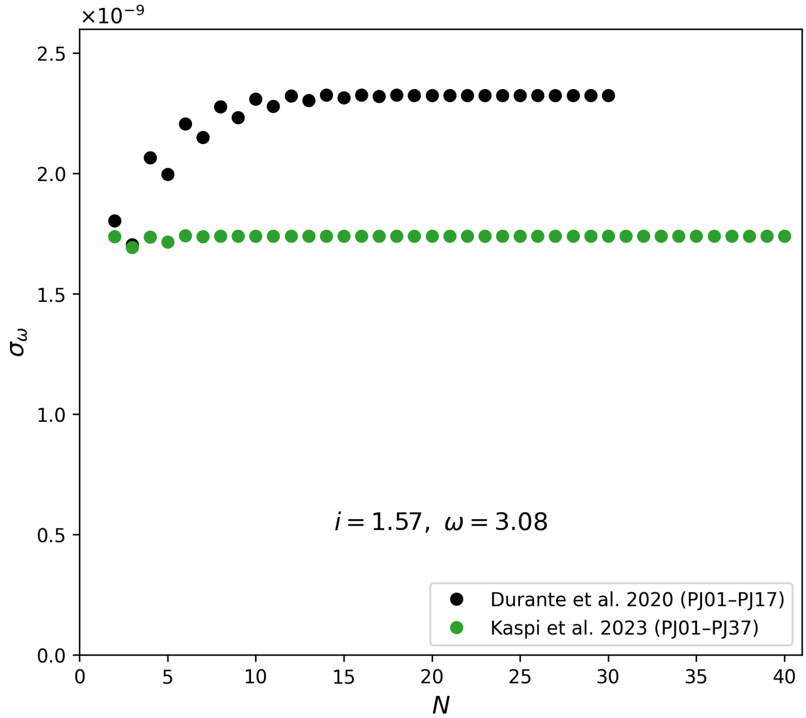

Figure 2. Basis-consistent propagated precession uncertainty plotted as a function of the maximum included harmonic degree N.

5.4 Dependence on orbital geometry

The propagated uncertainty varies across the (ω, i) plane because each orbital geometry responds differently to the same gravitational harmonics. Over the range

$$2.80 \le \omega \le 3.10, \qquad 1.55 \le i \le 1.75, \tag{5.5}$$

the Durante uncertainty ranges from 1.50×10^{-9} to 2.47×10^{-9}, while the updated uncertainty ranges from 1.38×10^{-9} to 1.84×10^{-9}. The improvement factor over this region ranges from approximately 1.09 to 1.36.

Evaluating the calculation at the realized perijove geometries included through PJ37 gives improvement factors between approximately 1.11 and 2.32, with a mean of approximately 1.57. The first-perijove value of 1.34 is therefore a useful benchmark but is not a universal property of the updated gravity solution. This geometry dependence should be retained when applying the method to individual orbital arcs or when constructing a future joint-orbit analysis.

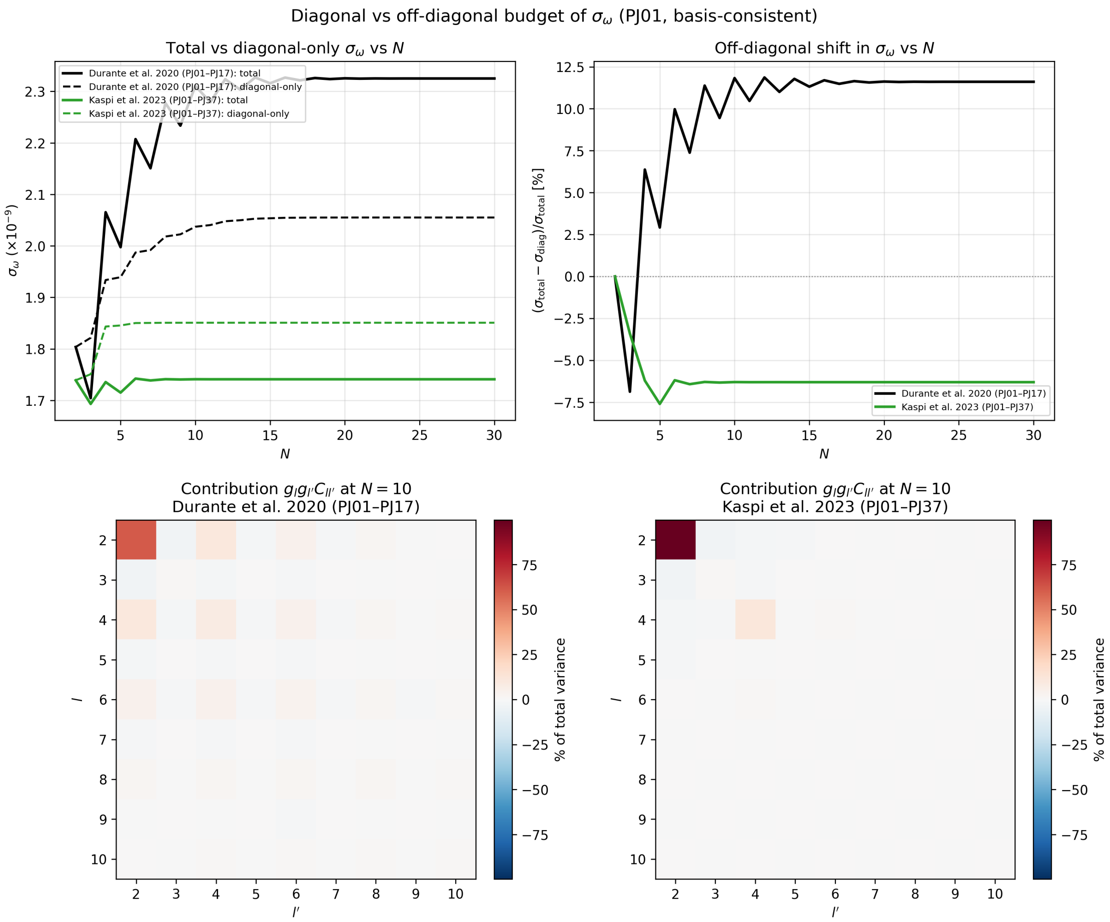

Figure 3. Decomposition of the basis-consistent propagated uncertainty into diagonal and correlated contributions. The upper panels compare total and diagonal-only standard deviations and show the signed off-diagonal shift. The lower panels show the signed contributions to the variance through $N = 10$.

6 Results

6.1 Updated precession uncertainty and fifth-force bound

At the minimum of the first-perijove plot, which we use to ensure consistency between our analysis and the previous literature, the basis-consistent propagated uncertainties are

$$\sigma_\omega^{\rm Durante} = 2.32 \times 10^{-9}, \tag{6.1}$$

$$\sigma_\omega^{\rm Kaspi} = 1.74 \times 10^{-9}. \tag{6.2}$$

Our updated result therefore reduces the precession uncertainty by a factor of

$$\frac{\sigma_\omega^{\rm Durante}}{\sigma_\omega^{\rm Kaspi}} \simeq 1.34. \tag{6.3}$$

Because the theoretical fifth-force response is not changed, the limiting value of $|\alpha|$ improves by almost the same factor at every λ.

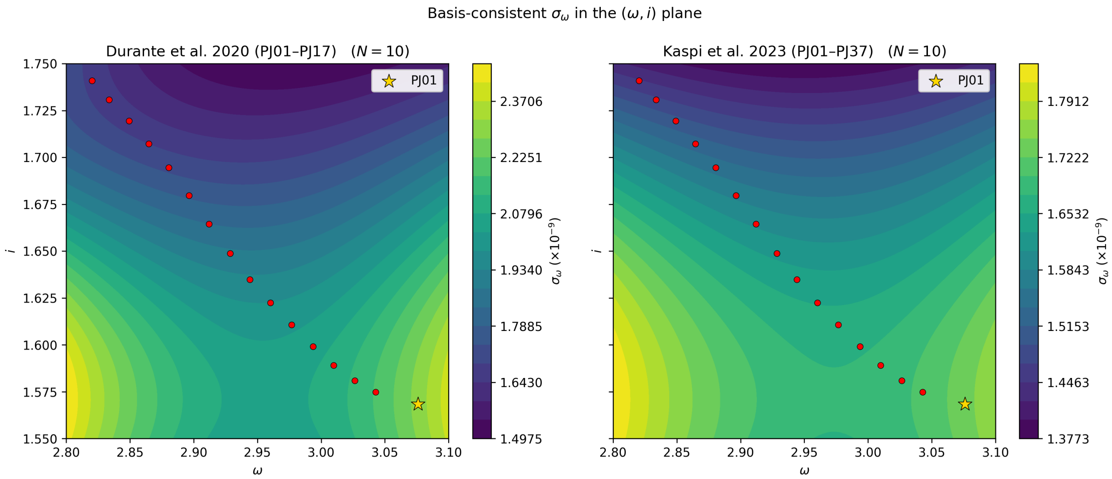

Figure 4. Basis-consistent precession uncertainty over the (ω, i) plane for the Durante gravity solution (left) and the re-derived covariance associated with the Kaspi solution (right). Red points mark observed perijoves, and the star marks PJ01.

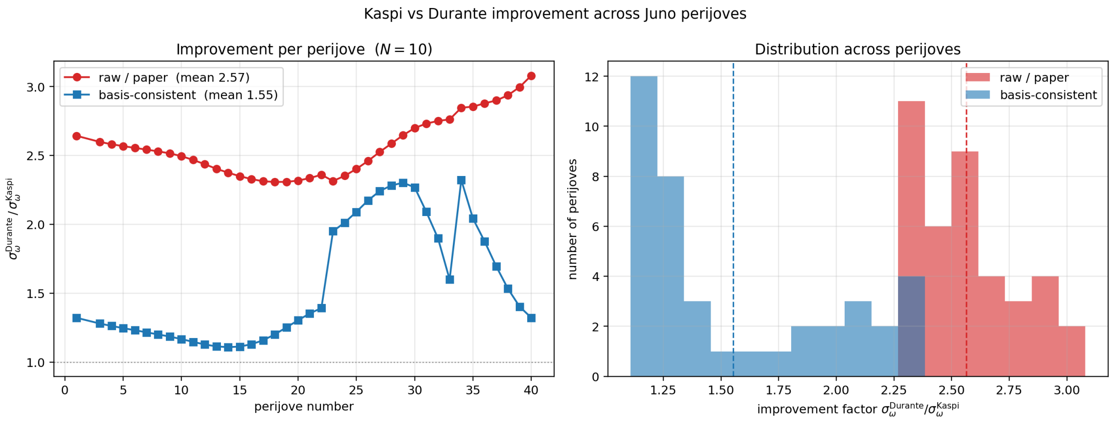

Figure 5. Improvement factor evaluated across all observed perijove geometries. The left panel shows improvement as a function of perijove number, and the right panel shows the distribution of improvement factors. The basis-consistent comparison is the blue series; the raw comparison is retained to contextualize the effect of normalization.

The strongest sensitivity occurs near

$$\lambda \simeq 1.35 \times 10^8 \text{ m}, \tag{6.4}$$

where the basis-consistent limits are approximately

$$|\alpha|_{95}^{\rm Durante} \simeq 2.98 \times 10^{-9}, \tag{6.5}$$

$$|\alpha|_{95}^{\rm Kaspi} \simeq 2.23 \times 10^{-9}. \tag{6.6}$$

At the range of greatest sensitivity, the updated covariance excludes fifth forces approximately 25% weaker than those excluded by the consistently re-evaluated Durante covariance.

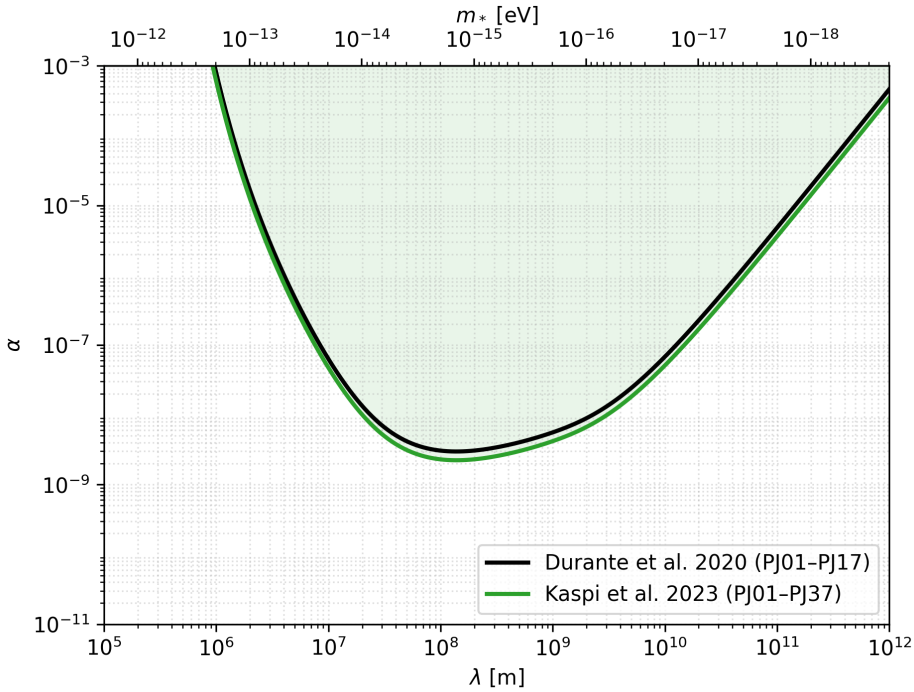

Figure 6. 95% C.L. constraint on the fifth-force strength parameter α as a function of force range parameter λ. The region above each curve is excluded. Note that the improvement appears mild due to the log axes.

7 Discussion

Several limitations remain. First, our constraint is obtained by propagating a published gravity covariance into the uncertainty of a single derived observable rather than by fitting a fifth-force contribution directly to the radio-tracking data, so any error introduced by the fit also reappears here. In addition, at the current significance level, our condition cannot definitively falsify a theory; it can only state that the theory is unlikely. However, this significance can be made arbitrarily low.

The gravity covariance is model-dependent because of the assumptions introduced by Kaspi et al. Although this is not numerically important because the high-degree terms make limited contributions, it is methodologically significant.

The fifth-force calculation assumes a static, spherically symmetric interaction whose source charge density is proportional to Jupiter's mass density, as well as a spherical Jupiter. To increase the precision of this result, a more detailed profile would be needed.

Juno continues to orbit Jupiter and remains in good health, so the analysis could be extended with more data. Although it is currently the only probe orbiting the planet, JUICE and Europa Clipper could be used to conduct a joint analysis once they approach Jupiter [2].

Acknowledgments

We thank Yohai Kaspi and Eli Galanti for useful correspondence. E.I. and A.L. acknowledge support from Brown University's Undergraduate Teaching and Research Awards (UTRA) program, and the authors thank the NASA Juno mission and Deep Space Network teams for collecting and analyzing the data underlying this work.

References

[1] S.J. Bolton et al., *The Juno mission*, *Space Science Reviews* **213** (2017) 5.

[2] P. Singh, S. Yan, I.J. Allali, J. Fan and L. Li, *The Juno mission as a probe of long-range new physics*, *Journal of High Energy Physics* **2025** (2025) 98 [2409.10616].

[3] D. Durante et al., *Jupiter's gravity field halfway through the Juno mission*, *Geophysical Research Letters* **47** (2020) e2019GL086572.

[4] Y. Kaspi, E. Galanti, R.S. Park, K. Duer, N. Gavriel et al., *Observational evidence for cylindrically oriented zonal flows on Jupiter*, *Nature Astronomy* **7** (2023) 1463.

[5] E. Fischbach and C. Talmadge, *Ten years of the fifth force*, *Proceedings of the 31st Rencontres de Moriond: Dark Matter and Cosmology, Quantum Measurements and Experimental Gravitation* (1996) [hep-ph/9606249].

[6] C.D. Carone and H. Murayama, *Possible light $U(1)$ gauge boson coupled to baryon number*, *Physical Review Letters* **74** (1995) 3122.

[7] R.N. Mohapatra and R.E. Marshak, *Local $B-L$ symmetry of electroweak interactions, majorana neutrinos and neutron oscillations*, *Physical Review Letters* **44** (1980) 1316.

[8] M. Escudero, D. Hooper, G. Krnjaic and M. Pierre, *Cosmology with a very light $L_\mu - L_\tau$ gauge boson*, *Journal of High Energy Physics* **2019** (2019) 71 [1901.02010].

[9] N. Blinov, S.A.R. Ellis and A. Hook, *Consequences of fine-tuning for fifth force searches*, *Journal of High Energy Physics* **2018** (2018) 29 [1807.11508].

[10] B. Militzer and W.B. Hubbard, *Study of jupiter's interior: Comparison of 2, 3, 4, 5, and 6 layer models*, *Icarus* **411** (2024) 115955.

[11] A. Milani, A.M. Nobili and P. Farinella, *Non-Gravitational Perturbations and Satellite Geodesy*, Adam Hilger, Bristol (1987).